High-Temperature Low-Cycle Fatigue Behavior of HS80H Ferritic–Martensitic Steel Under Dynamic Strain Aging

Wenlan Wei, Yaorong Feng, Lihong Han, Jianxun Zhang, and Hang Wang

In this work, low-cycle fatigue tests were performed on HS80H ferritic–martensitic steel with the strain amplitudes ranging from 0.5 to 2.0% at room temperature and 350 °C. The cyclic stress response at 350 °C was found to be different from that at room temperature due to the effect of dynamic strain aging and showed a significant secondary hardening when the strain values were 0.5 and 0.7%. Furthermore, the dynamic strain aging effect also resulted in an abnormal increase in fatigue life when the strain was 0.7%, which was due to the change in elastic strain. Additionally, the elastic strain and fatigue life were bilinear relations in the double logarithmic coordinates. Finally, the transmission electron microscope observations showed that the dynamic strain aging led to the change in substructure, while the grain was refined.

1. Introduction

Higher-strength Cr-Mo ferritic–martensitic steels, such as Cr-Mo, 9Cr-Mo and 10Cr-Mo steel, are extensively used at elevated temperatures, because of their good mechanical properties and creep resistance (Ref 1-4). HS80H steel is usually used in thermal recovery well casing in oil industry. The working mode of the thermal recovery well is as follows. First, the oil layer is heated by injecting high-temperature steam. Then, steam is repeatedly injected when the temperature drops to a certain extent (Ref 5-7). Due to complex stress conditions in the oil well, the displacement of casing materials is usually constrained, and the process of heating up produces considerable plastic strain. Therefore, the service environment of thermal cycling easily causes high-temperature low-cycle fatigue (LCF) damage to materials.

Dynamic strain aging (DSA) is mainly caused by the pinning effect of interstitial solid solution elements (Ref 8, 9). Within a certain temperature range, remarkable DSA effect occurs in the plastic deformation of metals or alloys (Ref 10-12). In addition, different solid solution elements show different sensitive temperatures to DSA. Alloy elements, such as Cr, Mo, Ni and Nb, considerably influence the temperature range of DSA. Ni-Co base superalloy experiences significant DSA effect within the temperature range of 350-500 °C (Ref 13). Meanwhile, the temperature range of DSA for Cr-Mo ferrite–martensitic steel is 260-450 °C (Ref 14). The operating temperature of HS80H steel lies within the temperature range of DSA, causing considerable influence on the mechanical properties of steel.

The LCF behavior of HS80H steel at room temperature indicates that the cyclic stress response increases at the initial stage of fatigue, which indicates a hardening, followed by the softening behavior until the specimen fractures. The cyclic stress responses also present the same characteristics from 0.4 to 2% strain (Ref 15). When the temperature is higher than 260 °C, the tensile curves of HS80H steel present Portevin–Le Chatelier (PLC) phenomenon, which represents the occurrence of DSA (Ref 16). Due to the effect of DSA at elevated temperatures, the cyclic stress response presents secondary hardening characteristics, causing changes in fatigue life and fracture mechanism. The effect of DSA on fatigue life and stress response is of considerable importance for the safety of material and has high research value. The fatigue life of ferritic–martensitic steel changes with temperature and considerably increases under the influence of DSA (Ref 17-21). It is worth mentioning that the DSA effect not only is related to temperature, but is also affected by strain. The magnitudes of strain amplitude are important factors in the occurrence of DSA (Ref 22-24).

The study of low-cycle fatigue behavior of ferritic–martensitic steel under the influence of DSA is nonexistent in the literature. In this paper, the effect of strain on the fatigue life of HS80H ferritic–martensitic steel at 350 °C is studied. Furthermore, the fatigue life and cyclic hardening, which are affected by DSA, are analyzed and discussed.

2. Experimental

The investigated material was HS80H tempered martensitic steel casing to be used for thermal recovery well. It underwent tempering treatment, which involves quenching at 890 °C for 30 min and, then, tempering at 650 °C for 2 h. The chemical components of the steel are listed in Table 1.

The specimens used for LCF tests were obtained from the casing along the axial direction, which is cylindrical with a diameter of 6 mm and a gauge of 12 mm, as shown in Fig. 1.

Wenlan Wei and **Jianxun Zhang**, State Key Laboratory for Mechanical Behavior of Materials, Xi'an Jiaotong University, Xi'an 710049, People's Republic of China; and **Yaorong Feng, Lihong Han**, and **Hang Wang**, State Key Laboratory of Performance and Structural Safety for Petroleum Tubular Goods and Equipment Materials, Xi'an 710065 Shaanxi, People's Republic of China. Contact e-mail: weiwenlannds@163.com.

Table 1 Chemical compositions (wt.%)

| C	Si	Mn	P	S	Cr	Mo	Ni	V	Ti	Cu
0.17	0.24	0.98	0.011	0.0034	0.99	0.33	0.059	0.029	0.013	0.021
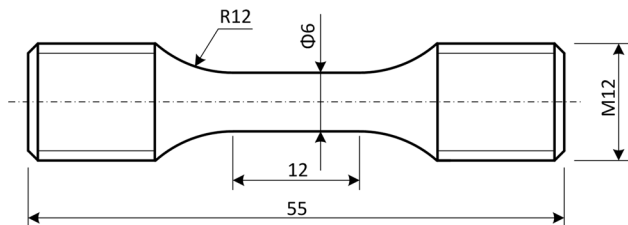
Fig. 1 Fatigue specimen geometry

The strain-controlled fatigue tests employing tension–compression fatigue loading were conducted using a closed loop servo-hydraulic testing machine (Instron 8862). A symmetric triangular strain time waveform was employed at a constant strain rate of 4×10^{-3} s^{-1}. The strain was measured using high-temperature ceramic extensometer having a 12-mm gauge. The accuracy of the extensometer is controlled using a PID system. The samples were divided into two groups, one of which was tested at room temperature and the other at 350 °C. The temperature is controlled using three temperature sensors near the sample in the heating furnace. The temperature variation did not exceed ± 1 °C. Additionally, LCF tests at strain amplitudes of 0.5, 0.7, 1.0, 1.5 and 2.0% under symmetric tension and compression loading conditions ($R = -1$) were conducted for each group. The tests were conducted twice at 350 °C to ensure the reproducibility of data.

After the LCF tests, fracture surfaces were subjected to ultrasonic cleaning in acetone solution. The fracture surface investigations were performed using scanning electron microscope with an acceleration voltage of 30 kV. Transmission electron microscope (TEM) was used to assess the evolution of dislocations and deformation behavior under LCF conditions at room temperature and 350 °C. The samples used for TEM were obtained through wire-electrode cutting and thinning them to 30-50 μm using sandpaper. Then, the samples were observed under TEM after twin-jet electropolishing.

3. Results

3.1 Cyclic Stress Response

The cyclic stress response curves at room temperature and 350 °C for HS80H under five different strain amplitudes are shown in Fig. 2. At room temperature, the cyclic stress response curves of different strain amplitudes present a similar variation trend, as shown in Fig. 2(a). The peak stress changed significantly in the few initial cycles. These changes, which were determined using strain amplitudes as hardening or softening, were different. Such changes gradually stabilized and, then, decreased with an increase in the number of cycles. Finally, the stress response rapidly decreased. At the initial stage of fatigue, the peak stress at 350 °C was similar to that at room temperature, whereas it changed unusually in the
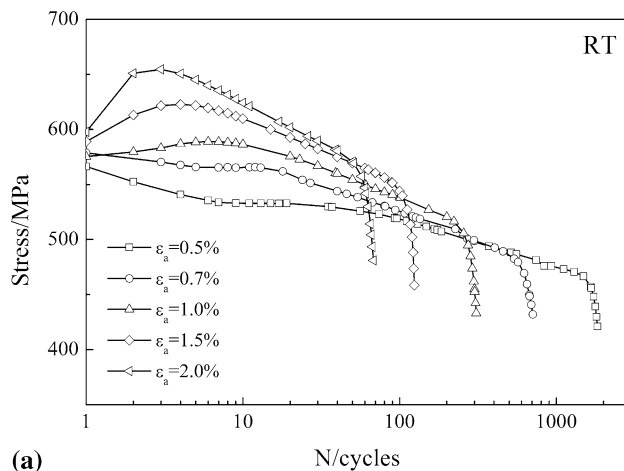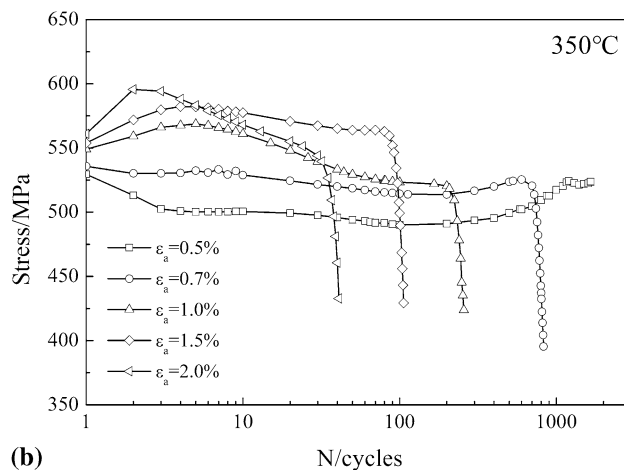
Fig. 2 Cyclic stress response curves of HS80H at (a) room temperature and (b) 350 °C as different strain amplitudes

following stage, as shown in Fig. 2(b). When the strain was 2, 1.5 or 1%, the stress response gradually decreased with an increase in the number of cycles, which indicates a typical softening process. However, the stress response gradually increased with an increase in the number of cycles when the strain was 0.7 or 0.5%, at which point the secondary hardening occurred. Notably, the final specimen at the end of the test fractured instantly when the strain was 0.5%. Meanwhile, rapid reduction in stress response did not occur.

The total cyclic stress response duration can be subdivided into three stages, as shown in Fig. 3. In the early stage of LCF, the peak stress reached the maximum value after a few cycles ($< 0.1N_f$) and, then, rapidly decreased (> 30 MPa) until it eventually stabilized. This stage was defined as the first stage ($0 < N < 0.25N_f$). Thereafter, the next stage was the steady change in the stress response (second stage). Whether the stress response increased or decreased, it was approximately linear with the increase in the number of cycles ($0.25N_f < N <$
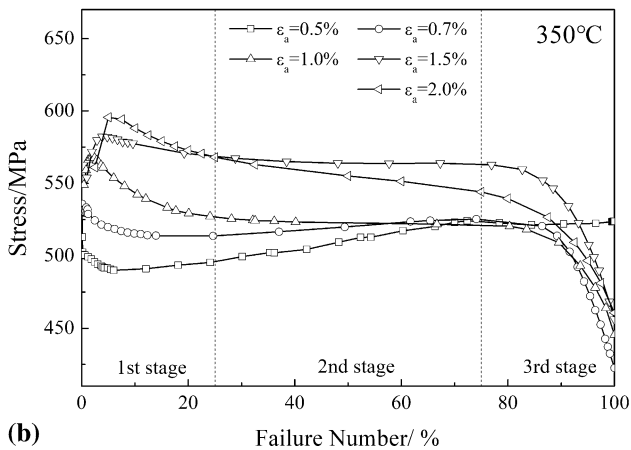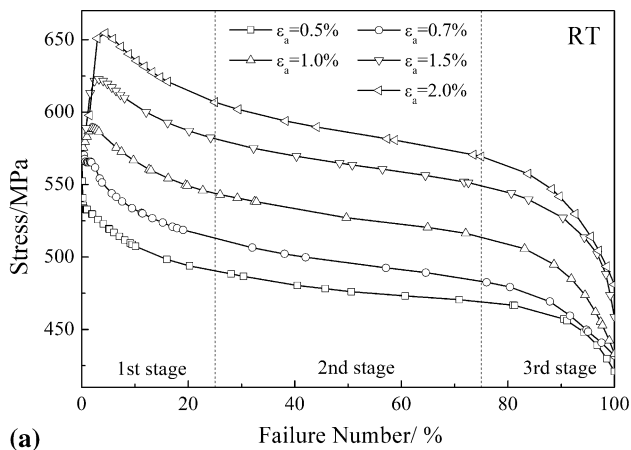
Fig. 4 Hardening coefficient of fatigue second stage at room temperature and 350 °C

Fig. 5 Strain–stress hysteresis loops at (a) RT and (b) 350 °C

Fig. 3 Cyclic stress response of HS80H showing three distinct stages at (a) room temperature and (b) 350 °C

$0.75N_f$). Then, the fatigue process entered the third stage ($0.75N_f < N < N_f$), and the peak stresses rapidly decreased due to crack propagation and deformation, which contributed to the instability of the specimen until it fractured. The stress response curve of 350 °C and 0.5% strain needs to be explained separately. Due to the secondary hardening, the third stage of the curve not only rapidly decreased, but also irregularly changed until the sudden fracture occurred.

The difference in cyclic stress response was mainly observed in the second stage of fatigue. The relationship between the cyclic stress response and number of cycles was approximately linear in the second stage. Therefore, the second stage of the cyclic stress response data was processed using linear regression. The slope of these data was obtained and represented the hardening coefficient k_h, which represents the variation of cyclic stress amplitude to describe the hardening and softening characteristics. Hardening is indicated by $k_h > 0$, while softening is represented by $k_h < 0$, as shown in Fig. 4. At room temperature, the second stage of fatigue was the softening process, and the rate of softening decreased with the increase in strain. At 350 °C, the second stage of fatigue was evidently the hardening process when the strain was 0.5 or 0.7%, while it was the softening process when the strain was 1.5 or 2%. When the strain was 1%, the value of k_h was approximately 0. The change in k_h with a decrease in strain was far larger than that at room temperature. This indicates that the cyclic stress response of HS80H steel at 350 °C is highly sensitive to different strains,
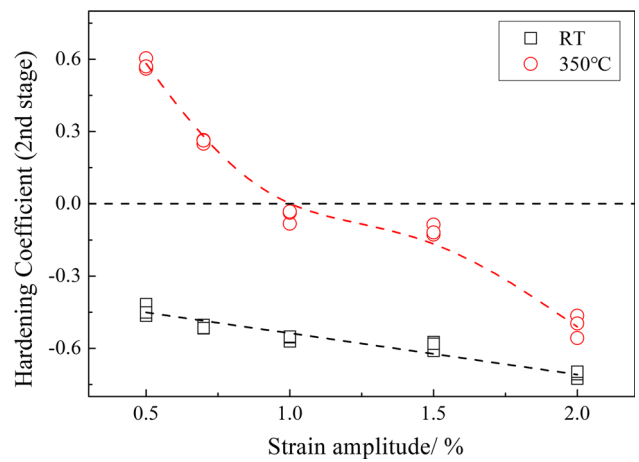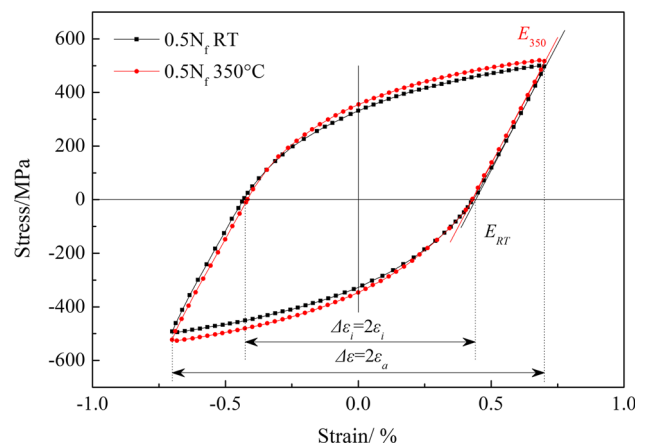
and the strengthening plasticity of the material exhibits considerable change.

3.2 High-Temperature Fatigue Life

The fatigue life of HS80H steel, represented by the number of cycles to failure (N_f), was evaluated under each testing condition in accordance with the standard ISO 12106-2017 (Ref 25). Then, the elastic (ε_e) and inelastic strain amplitudes (ε_i) were determined using the stabilized hysteresis loop at half-life in the second stage of fatigue, as shown in Fig. 5. The results are summarized in Table 2.

The Basquin's law describes the relationship between the stress amplitude and the number of stress reversals to failure in elastic stage (Ref 26):

$$\sigma_e = \sigma_f' \cdot \left(2N_f\right)^b \tag{Eq 1}$$

where σ_f' is the fatigue strength coefficient and b is the fatigue strength exponent.

Furthermore, the fatigue life and inelastic strain have an empirical relationship, which is given by the Manson–Coffin equation (Ref 27, 28):
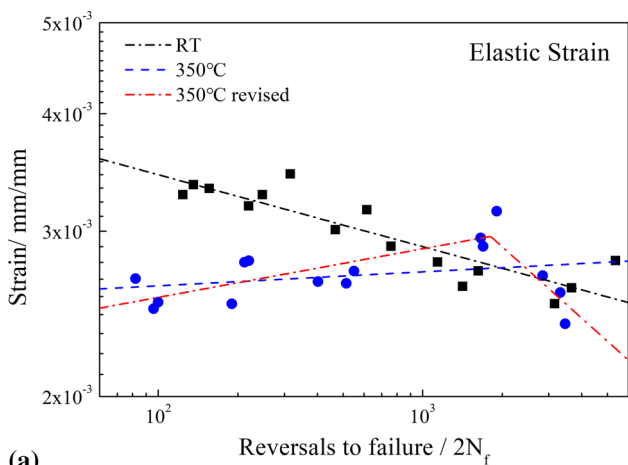
$$\varepsilon_i = \varepsilon_f' \cdot \left(2N_f\right)^c \tag{Eq 2}$$

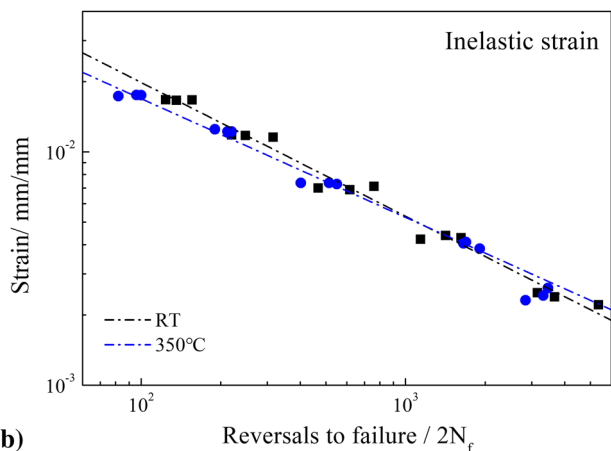where ε_f' is the fatigue ductility coefficient and c is the fatigue ductility exponent.

The fitting results of elastic and inelastic strain are presented in Fig. 6. Evidently, the results of inelastic strain at the two temperatures were almost similar to each other, indicating that the temperature did not obviously affect the characteristics of inelastic strain. However, the fitting results of elastic strain showed considerable deviations (Fig. 6a). The elastic strain and fatigue life usually presented a linear relationship in the double logarithmic coordinates, which confirmed the relationship at room temperature. At 350 °C, the elastic strain and fatigue life did not show a linear relationship in the double logarithmic coordinates. The fatigue life gradually increased with the increase in elastic strain. The elastic strain gradually decreased when the fatigue life was larger than 900, demonstrating an evident bilinear feature. According to the bilinear feature, the

Table 2 Test result of LCF for HS80H steels

	RT			350 °C		
ε_a, %	ε_i, %	ε_e, %	N_f, cycles	ε_i, %	ε_e, %	N_f, cycles
0.5	0.239	0.261	1832	0.242	0.258	1658
	0.249	0.251	1579	0.261	0.239	1730
	0.221	0.279	2686	0.231	0.269	1422
0.7	0.438	0.262	709	0.405	0.295	829
	0.422	0.278	570	0.411	0.289	847
	0.428	0.272	812	0.385	0.315	954
1	0.687	0.316	308	0.736	0.264	257
	0.699	0.301	234	0.728	0.272	275
	0.711	0.289	380	0.735	0.265	201
1.5	1.174	0.328	124	1.222	0.278	106
	1.181	0.319	110	1.249	0.251	95
	1.155	0.345	158	1.221	0.279	110
2	1.663	0.336	68	1.733	0.267	41
	1.672	0.328	62	1.752	0.248	48
	1.667	0.333	78	1.748	0.252	50

Table 3 LCF fitting coefficients of HS80H steel at room temperature and 350 °C

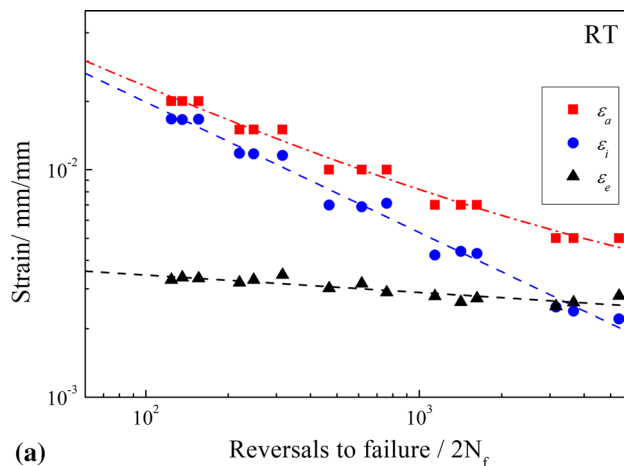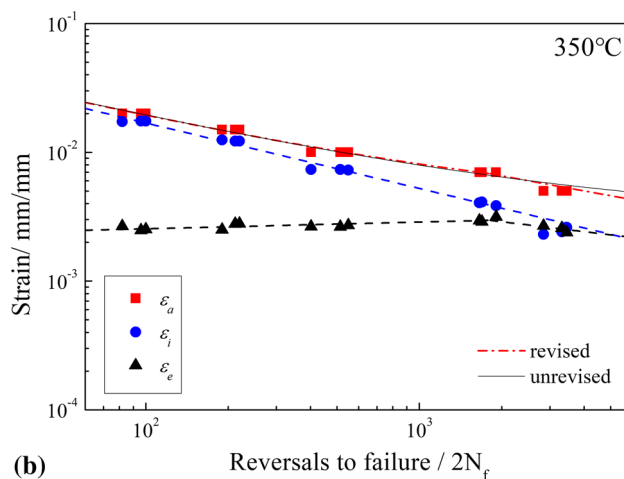| Temperature, °C	σ_f'	b	ε_f'	c
RT	976.5	− 0.0765	0.187	− 0.573
350 (before 908 cycles)	436.8	0.0517	0.124	− 0.509
350 (after 908 cycles)	3475.5	− 0.253	0.124	− 0.509

Fig. 6 Comparison of (a) elastic and (b) inelastic strain–life curves of HS80H steel at room temperature and 350 °C

Fig. 7 Strain–life curves of HS80H at (a) room temperature and (b) 350 °C

results of the two fatigue life intervals were fitted, and the results are shown in red in Fig. 6(a).

The empirical relationship between the fatigue life and the strain amplitude is obtained by adding the Basquin's law and the Manson–Coffin equation:

$$\varepsilon_a = \frac{\sigma'_f}{E}(2N_f)^b + \varepsilon'_f(2N_f)^c \qquad \text{(Eq 3)}$$

The test results were fitted according to the empirical formula (3), and the fitting coefficients are presented in Table 3. At 350 °C, the coefficient b was positive before 900 cycles, which was due to the increase in fatigue life with the elastic strain amplitudes. However, the behavior normalized after 900 cycles. The strain–life curve of HS80H steel is shown in Fig. 7(a) at room temperature. Figure 7(b) is the fatigue–life curve at 350 °C. The thin black solid line was fitted according to Eq 3. The red dash dot line resulted from the fitting of different intervals according to the bilinear characteristics. When the total strain was less than 0.7%, the life expectancy from Eq 3 was clearly larger than the actual fatigue life.

3.3 Dislocation Substructure

DSA affects not only the elastic strain, but also the characteristics of the cycle stress response. The secondary hardening is also due to the DSA, and the difference in dislocation substructure for the materials provides strong evidence. Figure 8 shows the TEM micrographs of the dislocations substructure of the different states of specimens.

The dislocation substructure of the untested sample is presented in Fig. 8(a). A large number of second phase precipitates and some diffused free dislocations were distributed in the lath subgrain. Additionally, precipitates were also observed at the subgrain boundary. Figure 8(b) shows the dislocation substructures when the number of cycles was $0.75N_f$ and the strain was 0.7% at room temperature. In the continuous softening stage of stress response (second stage), a large number of dislocations migrated and accumulated from grain to grain boundary. In addition, a few residual dislocations were found inside the grain. Meanwhile, the primary lath subgrain structures did not change, and a considerable amount of precipitates were still evident in the subgrain.

The dislocation substructure at 350 °C, which was completely different from that at room temperature, is shown in Fig. 8(c). The dislocation motion was affected by DSA, which led to the formation of new dislocation substructures. First, the pinning effect, caused by the DSA, slowed down the dislocation movement, which easily facilitated the formation of forest dislocation. In particular, the dislocation around the second phase precipitates can easily form atmospheres, which led to dislocation pile-up and the formation of dislocation walls. Then, the substructures were changed by numerous dislocation walls, and a smaller subgrain structure was formed. Figure 8(c) shows that the primary lath subgrain structures had transformed into smaller cellular substructures, and only a few of smaller precipitates were found in the subgrain. A large number of dislocation pile-ups appeared at the new subgrain boundary. Furthermore, smaller size corresponded to higher strength
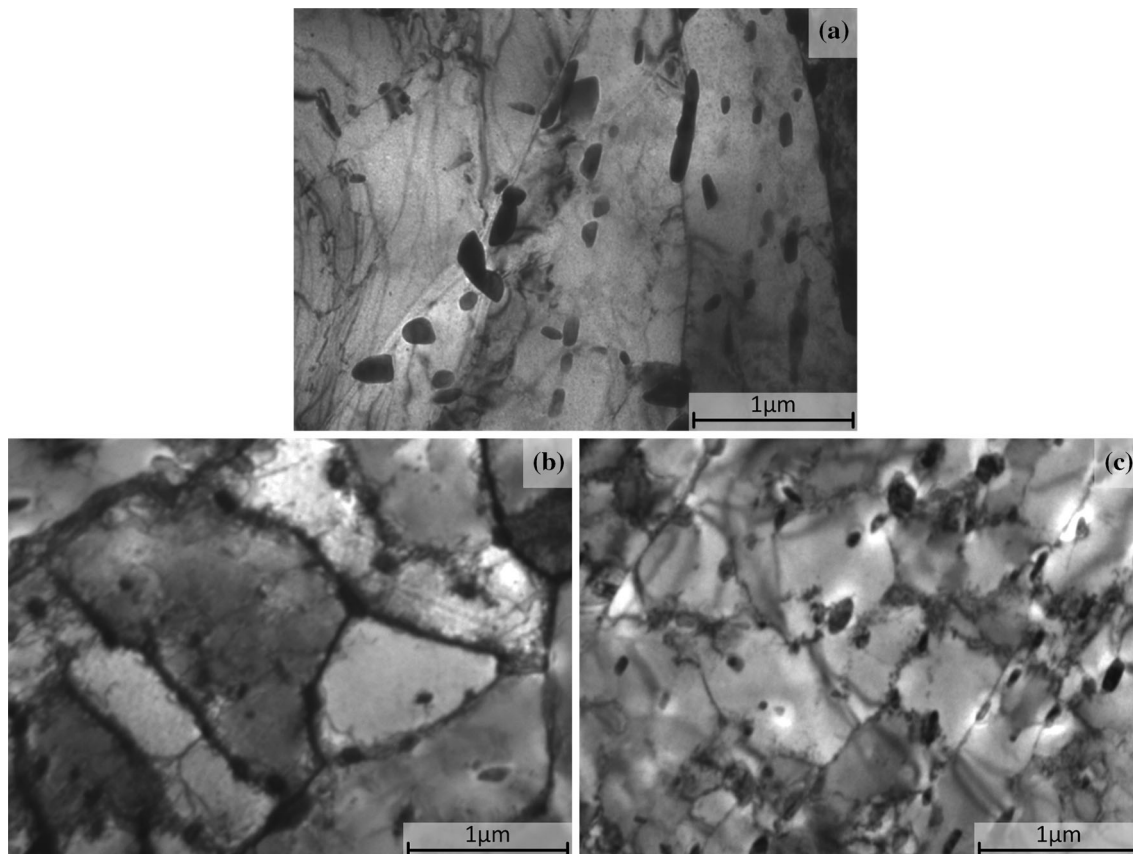

Fig. 8 TEM micrographs of dislocation substructure in (a) untested and after LCF testing in which the number of cycles is $0.75N_f$ and the strain is 0.7% at (b) room temperature and (c) 350 °C

under the condition of no phase transition (Ref 29-31). DSA led to the continuous refinement of grain during LCF. Therefore, the cycle stress response evidently showed hardening characteristics. Meanwhile, due to the influence of DSA, the interaction of precipitates with dislocations near the new subgrain boundary enhanced the new substructures and stabilized them. The crack propagation was inhibited by the new structure, which prolonged the fatigue life.

4. Discussion

For the LCF life at elevated temperature, previous studies have shown that the fatigue life reduced under the influence of elevated temperature due to changes in strain characteristics (Ref 32-35). The ratio of elastic strain to total strain reduced at elevated temperature, and an increase in inelastic strain led to the acceleration of fatigue damage, thereby reducing the fatigue life (Ref 36).

The test results of HS80H steel obviously differed from those of previous studies. Figure 9(a) shows the relationship between the total strain and its elastic strain. At room temperature, the elastic strain monotonously increased with the increase in total strain. However, the results at 350 °C demonstrated that the elastic strain initially increased and then,
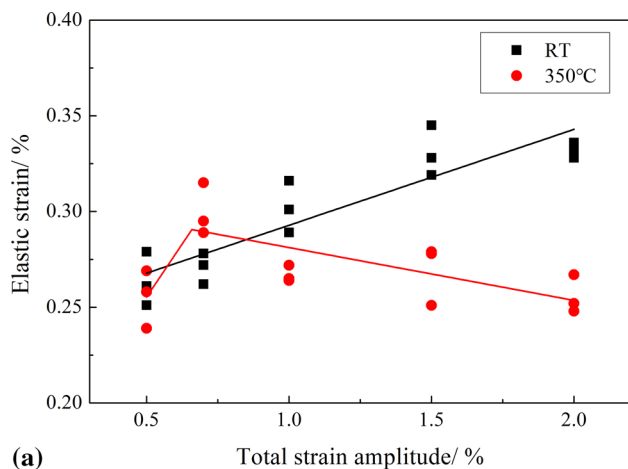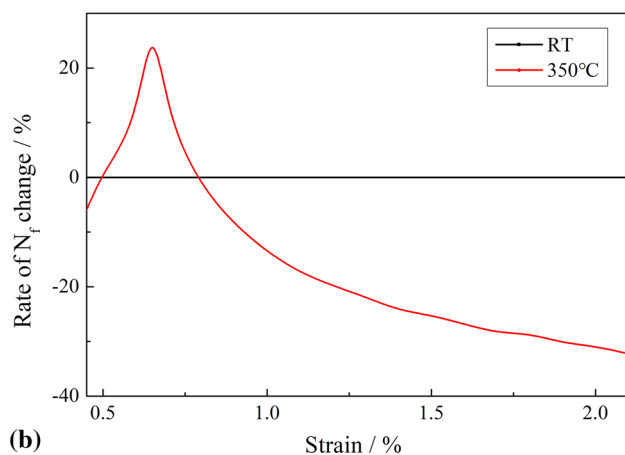
decreased. The peak appeared when the total strain was within the range of 0.5-1%. Particularly, when the strain was 0.7%, the elastic strain at 350 °C was evidently higher than that at room temperature. In other words, the increased elastic strain reduced the inelastic strain, which decreased the fatigue damage caused by a single cycle. The number of cycles needed to accumulate sufficient damage increased. Therefore, the fatigue life of the material under this condition was higher than that at room temperature. The relationship between the fatigue life at room temperature and that at 350 °C is shown in Fig. 9(b). The fitting results of fatigue life at room temperature were used as the standard fatigue life, which were represented by a straight line of y = 0. Furthermore, the relationship between the fitting results at fatigue life of 350 °C and that at room temperature is represented by the rate of N_f change ($[N_{350}/N_{RT} - 1]100\%$), as shown in Fig. 9(b). The fatigue life of fitting results at 350 °C was 20% higher than that at room temperature when the strain was 0.65%. The peak value also appeared which agreed with the variation trend of elastic strain.

The previous study showed that a significant DSA existed between the temperatures of 260 and 450 °C for HS80H steel (Ref 12, 16). DSA is a strengthening phenomenon in metals and alloys and is caused by the interaction between the diffusive solute atoms and the moving dislocation. The solid solution elements of HS80H steel, such as C, Cr, Mo, Ni, and V, tend to segregate dislocations and form pinning effects. According to the model proposed by RE Reed Hill (Ref 37, 38), when the material has DSA during plastic deformation, the rheological stress σ_t will be composed of two independent parts. The first is σ in the absence of DSA, and the second is σ_{DSA} in the presence of DSA.

$$\sigma_t = \sigma + \sigma_{DSA} \tag{Eq 4}$$

Under the influence of DSA, the rheological stress of HS80H steel considerably increased under specific conditions (temperature of 350 °C and strain of 0.7%). Moreover, the elastic modulus at 350 °C did not change compared to that at room temperature, as shown in Fig. 5. Therefore, the ratio of elastic strain to total strain increased, implying that the fatigue life had prolonged.

5. Conclusions

The LCF behavior of HS80H steel at room temperature and 350 °C was studied in cyclic stress response, fatigue life and micro-substructure, which led to the following conclusions.

- The cyclic stress response shows secondary hardening characteristics when the temperature is 350 °C and the strain is less than 1.0%.
- The DSA exerts a significant effect on the fatigue life of HS80H steel at 350 °C. The elastic strain and fatigue life present a bilinear feature in the double logarithmic coordinate system.
- The proportion of elastic strain in total strain at elevated temperature markedly changes due to the presence of DSA, which affects the accumulation of plastic damage and considerably changes the LCF life.
- The micro-substructure is transformed from lamellar subgrains to smaller cellular subgrains at 350 °C.

(a)

(b)

Fig. 9 Relationship of (a) elastic/total strain and (b) 350 °C/RT fatigue life

References

1. A.Y. Churyumov, M.G. Khomutov, A.N. Solonin, A.V. Pozdniakov, T.A. Churyumova, and B.F. Minyaylo, Hot Deformation Behaviour and Fracture of 10CrMoWNb Ferritic–Martensitic Steel, *Mater. Des.*, 2015, **74**, p 44–54

2. J. Nikitin, S. Schoch, and A.M. Freund, Effect of Silicon on the Microstructure and Mechanical Properties of Reduced Activation Ferritic/Martensitic Steel, *J. Nucl. Mater.*, 2015, **459**(7), p 13–19

3. X. Gong, E. Stergar, P. Marmy, S. Gavrilov, X. Gong, E. Stergar, P. Marmy, S. Gavrilov, X. Gong, and E. Stergar, Tensile Fracture Behavior of Notched 9Cr-1Mo Ferritic–Martensitic Steel Specimens in Contact with Liquid Lead-Bismuth Eutectic at 350 °C, *Mater. Sci. Eng. A*, 2017, **692**, p 139–145

4. A. Nagesha, M. Valsan, R. Kannan, K.B.S. Rao, and S.L. Mannan, Influence of Temperature on the Low Cycle Fatigue Behaviour of a Modified 9Cr-1Mo Ferritic Steel, *Int. J. Fatigue*, 2002, **24**(12), p 1285–1293

5. A.K. Ambastha, Thermal Recovery Well Test Design and Interpretation, *SPE Form. Eval.*, 1989, **4**(4), p 173–180

6. R. Lin, D. Song, X. Wang, and D. Yang, Experimental Determination of In Situ Hydrogen Sulfide Production during Thermal Recovery Processes, *Energy Fuels*, 2016, **30**(7), p 5323–5329

7. J.S. Jeon, S.R. Lee, L. Pasquinelli, and I.L. Fabricius, Sensitivity Analysis of Recovery Efficiency in High-Temperature Aquifer Thermal Energy Storage with Single Well, *Energy*, 2015, **90**(3), p 1349–1359

8. M.A. Soare and W.A. Curtin, Single-Mechanism Rate Theory for Dynamic Strain Aging in fcc Metals, *Acta Mater.*, 2008, **56**(15), p 4091–4101

9. C.S. Seok and K.L. Murty, Effect of Dynamic Strain Aging on Mechanical and Fracture Properties of A516Gr70 Steel, *Int. J. Press. Vessels Pip.*, 1999, **76**(14-15), p 945–953

10. S.G. Hong and S.B. Lee, The Tensile and Low-Cycle Fatigue Behavior of Cold Worked 316L Stainless Steel: Influence of Dynamic Strain Aging, *Int. J. Fatigue*, 2004, **26**(8), p 899–910

11. D. Wagner, J.C. Moreno, and C. Prioul, Dynamic Strain Aging Sensitivity of Heat Affected Zones in C-Mn Steels, *J. Nucl. Mater.*, 1998, **252**(3), p 257–265

12. K. Mariappan, V. Shankar, R. Sandhya, G.V.P. Reddy, and M.D. Mathew, Dynamic Strain Aging Behavior of Modified 9Cr-1Mo and Reduced Activation Ferritic Martensic Steels Under Low Cycle Fatigue, *J. Nucl. Mater.*, 2013, **435**(1-3), p 207–213

13. C.Y. Cui, Y.F. Gu, Y. Yuan, and H. Harada, Dynamic Strain Aging in a New Ni-Co Base Superalloy, *Scr. Mater.*, 2011, **64**(6), p 502–505

14. W. Karlsen, M. Ivanchenko, U. Ehrnstén, Y. Yagodzinskyy, and H. Hänninen, Microstructural Manifestation of Dynamic Strain Aging in AISI, 316 Stainless Steel, *J. Nucl. Mater.*, 2009, **395**(1-3), p 156–161

15. W. Wei, L. Han, H. Wang, J. Wang, J. Zhang, Y. Feng, and T. Tian, Low-Cycle Fatigue Behavior and Fracture Mechanism of HS80H Steel at Different Strain Amplitudes and Mean Strains, *J. Mater. Eng. Perform.*, 2017, **26**(4), p 1717–1725

16. W. Wei, L. Han, J. Wang, W. Hang, and Y. Feng, High Temperature Mechanical Properties of 10Cr3Mo and N80 Steels, *Heat Treat. Met.*, 2016, **41**(2), p 23–27

17. V.S. Srinivasan, R. Sandhya, M. Valsan, K.B.S. Rao, S.L. Mannan, and D.H. Sastry, The Influence of Dynamic Strain Ageing on Stress Response and Strain–Life Relationship in Low Cycle Fatigue of 316L(N) Stainless Steel, *Scr. Mater.*, 1997, **37**(10), p 1593–1598

18. C. Ye, S. Suslov, B.J. Kim, E.A. Stach, and G.J. Cheng, Fatigue Performance Improvement in AISI, 4140 Steel by Dynamic Strain Aging and Dynamic Precipitation During Warm Laser Shock Peening, *Acta Mater.*, 2011, **59**(3), p 1014–1025

19. H.W. Zhou, Y.Z. He, H. Zhang, and Y.W. Cen, Influence of Dynamic Strain Aging Pre-treatment on the Low-Cycle Fatigue Behavior of Modified 9Cr-1Mo Steel, *Int. J. Fatigue*, 2013, **47**(1), p 83–89

20. Z. Huang, D. Wagner, and C. Bathias, Some Metallurgical Aspects of Dynamic Strain Aging Effect on the Low Cycle Fatigue Behavior of C-Mn Steels, *Int. J. Fatigue*, 2015, **80**(3), p 113–120

21. M.S. Pham and S.R. Holdsworth, Role of Microstructural Condition on Fatigue Damage Development of AISI, 316L at 20 and 300 & #xB0;C, *Int. J. Fatigue*, 2013, **51**, p 36–48

22. M. Koyama, T. Sawaguchi, and K. Tsuzaki, Selective Appearance of ε-Martensitic Transformation and Dynamic Strain Aging in Fe-Mn-C Austenitic Steels, *Phil. Mag.*, 2012, **92**(24), p 3051–3063

23. M. Koyama, T. Sawaguchi, and K. Tsuzaki, Influence of Dislocation Separation on Dynamic Strain Aging in a Fe-Mn-C Austenitic Steel, *Mater. Trans.*, 2012, **53**(3), p 546–552

24. J. Cheng and S. Nemat-Nasser, A Model for Experimentally-Observed High-Strain-Rate Dynamic Strain Aging in Titanium, *Acta Mater.*, 2000, **48**(12), p 3131–3144

25. Institution BS. Iso/cd 12106 - Metallic Materials - Fatigue Testing Axial Strain - Controlled Method

26. O.H. Basquin, *The Exponential Law on Endurance Tests*, Vol 10, ASTM, West Conshohocken, 1910

27. L.F.J. Coffin, A Study of the Effects of Cyclic Thermal Stresses on a Ductile Metal, *Rheumatism*, 1953, **22**(6), p 419–606

28. S.S. Manson, Behavior of Materials Under Conditions of Thermal Stress, *Techn. Rep. Arch. Image Libr.*, 1954, **7**(s3-4), p 661–665

29. R. Klinman, G.R. Webster, F.J. Marsh, and E.T. Stephenson, Ultrasonic Prediction of Grain Size, Strength, and Toughness in Plain Carbon Steel, *Mater. Eval.*, 1980, **38**(10), p 26–32

30. N.J. Petch, The Influence of Grain Boundary Carbide and Grain Size on the Cleavage Strength and Impact Transition Temperature of Steel, *Acta Metall.*, 1986, **34**(7), p 1387–1393

31. P.H. Chang and A.G. Preban, The Effect of Ferrite Grain Size and Martensite Volume Fraction on the Tensile Properties of Dual Phase Steel, *Acta Metall.*, 1985, **33**(5), p 897–903

32. J. Polák, M. Klesnil, and J. Helešic, Cyclic Stress–Strain Response of 2 1/4Cr-1 Mo Steel at Elevated Temperatures, *Fatigue Fract. Eng. Mater. Struct.*, 2010, **9**(3), p 185–194

33. G.G. Al-Khateeb and K.A. Ghuzlan, The Combined Effect of Loading Frequency, Temperature, and Stress Level on the Fatigue Life of Asphalt Paving Mixtures Using the IDT Test Configuration, *Int. J. Fatigue*, 2014, **59**(3), p 254–261

34. B. Vieille and W. Albouy, Fatigue Damage Accumulation in Notched Woven-Ply Thermoplastic and Thermoset Laminates at High-Temperature: Influence of Matrix Ductility and Fatigue Life Prediction, *Int. J. Fatigue*, 2015, **80**, p 1–9

35. L. Straßberger, A. Chauhan, T. Gräning, S. Czink, and J. Aktaa, High-Temperature Low-Cycle Fatigue Behavior of Novel Austenitic ODS Steels, *Int. J. Fatigue*, 2016, **93**, p 194–200

36. D. Lefebvre and F. Ellyin, Cyclic Response and Inelastic Strain Energy in Low Cycle Fatigue, *Int. J. Fatigue*, 1984, **6**(1), p 9–15

37. K.W. Qian and R.E. Reed-Hill, A Model for the Flow Stress and Strain Rate Sensitivity of a Substitutional Alloy—Cu-3.1 at.% Sn, *Acta Metall.*, 1983, **31**(1), p 87–94

38. R.E. Reedhill and T. Zhu, A Model for the Flow Stress and Strain Rate Sensitivity in a Refractory Metal, *High Temp. Mater. Process. (London)*, 1984, **6**(1-2), p 93–117